ACS Energy LETTERS

http://pubs.acs.org/journal/aelccp

LETTER

Asymmetric Bipolar Membrane for High Current Density Electrodialysis Operation with Exceptional Stability

Éowyn Lucas,[‡] Justin C. Bui,[‡] Timothy Nathan Stovall, Monica Hwang, Kaiwen Wang, Emily R. Dunn, Ellis Spickermann, Lily Shiau, Ahmet Kusoglu, Adam Z. Weber, Alexis T. Bell, Shane Ardo, Harry A. Atwater,* and Chengxiang Xiang*

Cite This: *ACS Energy Lett.* 2024, 9, 5596−5605

Read Online

ACCESS | Metrics & More | Article Recommendations | Supporting Information

ABSTRACT: **Bipolar membranes (BPMs) enable isolated acidic/alkaline regions in electrochemical devices, facilitating optimized environments for electrochemical separations and catalysis. For economic viability, BPMs must attain stable, high current density operation with low overpotentials in a freestanding configuration. We report an asymmetric, graphene oxide (GrOx)-catalyzed BPM capable of freestanding electrodialysis operation at 1 A cm^{-2} with overpotentials <250 mV. Use of a thin anion-exchange layer improves water transport while maintaining near unity Faradaic efficiency for acid and base generation. Voltage stability exceeding 1100 h with an average drift of 70 μV/h at 80 mA cm^{-2} and 100 h with an average drift of −300 μV/h at 500 mA cm^{-2} and implementation in an electrodialysis stack demonstrate real-world applicability. Continuum modeling reveals that water dissociation in GrOx BPMs is both catalyzed and electric-field enhanced, where low pK_a moieties on GrOx enhance local electric fields and high pK_a moieties serve as active sites for surface-catalyzed water dissociation. These results establish commercially viable BPM electrodialysis and provide fundamental insight to advance design of next-generation devices.**

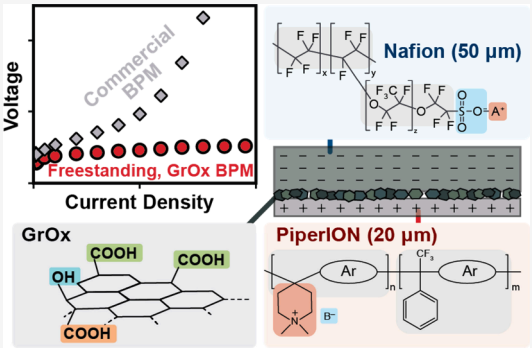

Electrochemical technologies designed for water electrolysis,[1−4] CO_2 conversion,[5,6] and carbon removal[6−9] are critical for making progress toward a sustainable future.[10−12] Bipolar membranes (BPMs) that demonstrate stable, high current-density operation under reverse bias have immense promise for implementation in such devices, due to their ability to sustain separated acidic and alkaline environments in a single device. The ability to sustain gradients in pH facilitates optimal cathode and anode environments for electrocatalysis, capable of attaining high activity, selectivity, and stability with earth-abundant elements.[13−19] BPMs have also shown promise when integrated in electrodialysis cells used for pH-swing direct air capture (DAC),[20−22] extraction of dissolved inorganic carbon from oceanwater in direct ocean capture (DOC), and ocean alkalinity enhancement.[6,9,23] Techno-economic analysis has shown that the primary cost-drivers of these systems are energy costs and membrane replacement.[24] Hence, stable operation at high current densities (~1 A cm^{-2}) and low voltages (<1.5 V) is critical to enable economical BPM electrolysis, electrodialysis, and environmental remediation processes.[25,26]

BPMs are comprised of a cation exchange layer (CEL) laminated to an anion-exchange layer (AEL) with a water dissociation (WD) catalyst dispersed within the CEL-AEL junction (i.e., the BPM catalyst layer (CL)).[27] In the BPM CL, protons and hydroxides from the CEL and AEL react to form water, neutralizing mobile ions to generate a space−charge depletion region of just a few nanometers, resulting in a strong electric field on the order of 10^8 to 10^9 V m^{-1}.[28,29] Under reverse bias, electric fields present in the BPM CL accelerate WD via the Second Wien Effect and the presence of the catalyst increases the rate of WD, potentially through further screening of the electric field, or by providing alternative, catalyzed pathways for WD.[30] These combined effects generate separated H^+ and OH^- and establish ionic currents that enable

Received: June 20, 2024
Revised: September 21, 2024
Accepted: September 26, 2024
Published: October 28, 2024

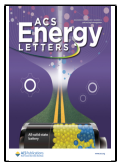

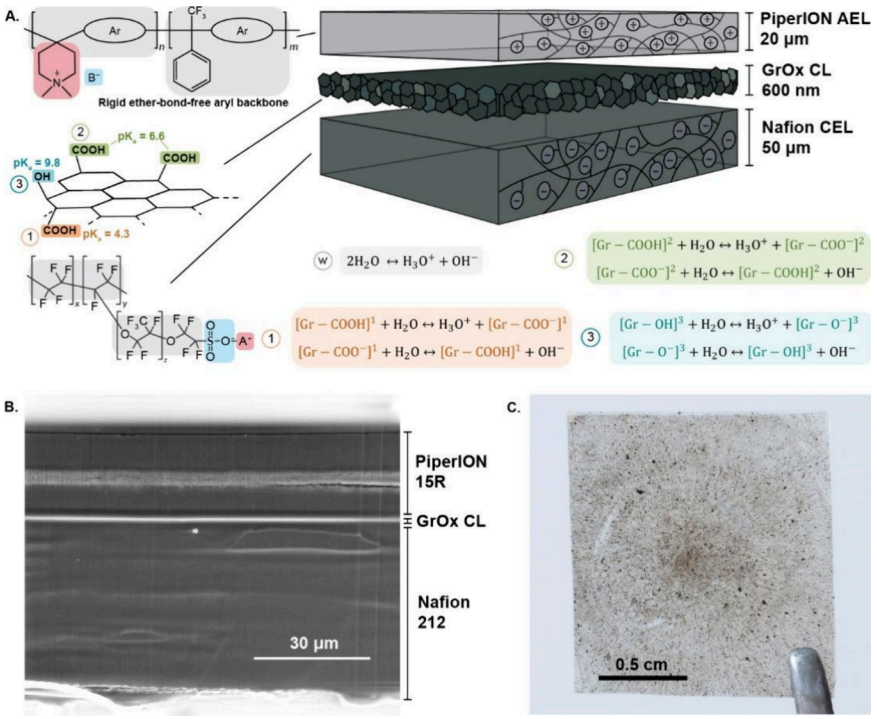

Figure 1. GrOx catalyzed, asymmetric BPM design. (A) Schematic of each layer of the BPM, indicating thickness and chemical structure. For the GrOx CL, the sites (1, 2, and 3) that contribute to WD enhancement are labeled with their pK_a values and the relevant WD enhancement reactions. (B) SEM cross section of the BPM layers. The lighter region in the AEL is a mechanical support layer. (C) Picture of assembled BPM.[50]

buildup of pH gradients across the BPM.[31−34] Existing commercial BPMs (e.g., Fumasep FBM, ASTOM BPM) are limited to stable operation at current densities up to ∼100 mA cm^{-2}, as the rate of water transport through the BPM cannot match that of WD at higher current densities.[27,28,35]

To address these challenges, substantial research has been devoted to the development of BPMs capable of achieving high current densities and low overpotentials in membrane electrode assembly (MEA) systems for electrolysis and energy conversion, where the mechanical pressure from the electrodes directly contacting the BPM helps to maintain its mechanical integrity.[36−38] However, in the production of acid and base via electrodialysis, critical to many applications such as wastewater treatment, metal recovery, and direct ocean capture of CO_2, physical separation between the electrodes and the BPM is required to facilitate the sustained generation of disparate electrolyte environments.[30] Unfortunately, BPMs capable of operating without added mechanical compression (i.e., freestanding BPMs) have not yet achieved the high current densities and efficiencies demonstrated by BPMs in compressed MEAs. Hence, there is great need for freestanding BPMs capable of active, efficient, and stable operation.

To increase the achievable rates for freestanding BPMs, recent efforts have improved performance by ameliorating water transport limitations with thinner CELs or AELs that increase water transport to the junction, achieving current densities on the order of 1 A cm^{-2}.[17,39] However, these asymmetric BPMs have not yet achieved the required metrics for commercial feasibility, necessitating further research. Additionally, to achieve industrially relevant rates of WD with minimal applied voltage, BPMs must not only overcome water transport limitations, but also increase the rate of WD at a given applied potential. This objective can be achieved by engineering the WD CL. A range of catalyst materials, such as polymers, metal oxides, and buffer materials have been examined experimentally for WD enhancement.[27,38,40] Previous work predicts that the concentration of ionizable sites in the CEL, AEL, and CL, along with the specific pK_a values of the catalyst sites, directly affects the rate of WD at the BPM junction.[27,28,38,41,42] Neither theory nor experiments, however, have been able to determine explicitly which WD enhancement pathway dominates, leaving open a critical area for further investigation.[27,43−45]

Despite the substantial enhancements in polymer and catalyst materials for improving water transport and enhancing WD, freestanding BPMs suffer from a substantial lack of long-term stability.[27,28] Beyond voltage requirements for WD, stability must be improved to mitigate membrane replacement in BPM electrodialysis systems. Additionally, enhanced adhesion between the AEL, CL, and CEL is necessary to enable the freestanding operation required for electrodialysis. Recent work has sought to address this challenge by creating complex junction morphologies to improve catalytic surface area and mechanical stability, however these complex morphologies require additional chemical processing steps, and few have been able to achieve low overpotentials at industrially relevant current densities and stability.[17,39,43,46] In principle, an idealized freestanding BPM should integrate a catalyst layer that exhibits high activity while simultaneously providing robust mechanical integrity.

Herein, we report a BPM comprised of a Nafion 212 CEL (∼50 μm), a thin PiperION A15R AEL (∼20 μm), and a graphene oxide (GrOx) WD catalyst (layer thickness 200−1000 nm) (Figure 1) that is stable at current densities up to 1 A cm^{-2} when tested under reverse bias in a custom-made, 5-chamber electrodialysis flow cell (Figure S1). The BPM is easy

https://doi.org/10.1021/acsenergylett.4c01662
ACS Energy Lett. 2024, 9, 5596−5605

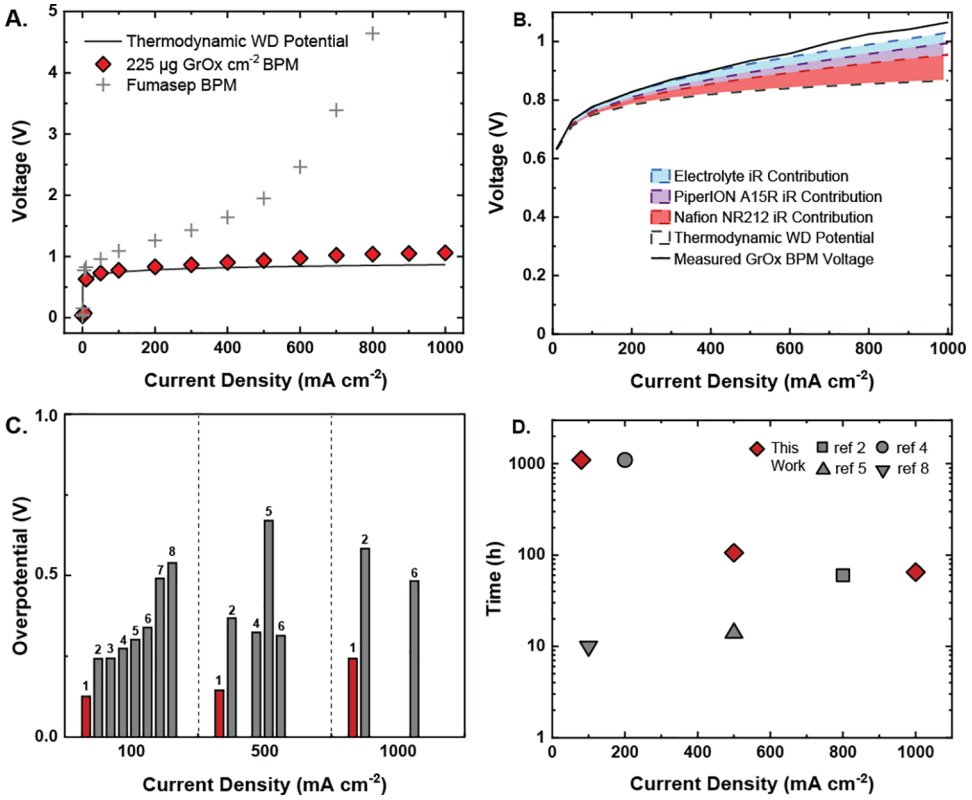

Figure 2. GrOx catalyzed, asymmetric BPM performance. (A) Polarization curves for the best performing BPM (225 μg cm^{-2} GrOx loading) and the commercial Fumasep BPM, tested in a custom electrodialysis cell, compared to the thermodynamic potential for WD. (B) Sum of voltage contributions due to WD potential, CEL ohmic losses, AEL ohmic losses, electrolyte ohmic losses, and WD kinetics compared to measured performance of the BPM. Comparison of the (C) overpotentials at 100, 500, and 1000 mA cm^{-2} and (D) operation in hours at various current densities for the best performing BPM to other reported freestanding BPMs (Table S1).[2,13,17,38−40,43,45,46,51] In panels C and D, various BPMs across the literature are compared, and the labeling of each bar or marker corresponds to the numbering in Table S1. Details regarding the calculations of overpotential and stability are enumerated in the Supporting Information Section S2.

to fabricate, due to intrinsic adhesion between a GrOx-coated Nafion CEL and the Versogen AEL. We investigated the voltage and overpotential at various current densities, optimal catalyst loading, operation over extended periods (>60 h), adhesion, the effect of increasing the CL active area, and Faradaic Efficiency (FE) of the BPM. Applied voltage analysis reveals that the BPM operates at just above the thermodynamic minimum necessary for WD, with an incredibly low overpotential of <250 mV at 1 A cm^{-2}. This result indicates that the GrOx catalyst increases the rate of WD at a given applied potential, and that the choice of a thin AEL facilitates achievement of high current densities by improving water transport to the CL.

The reported BPM is capable of operation in a freestanding flow environment for >1100 h at 80 mA cm^{-2}, >100 h at 500 mA cm^{-2}, and >60 h at 1 A cm^{-2}. Moreover, the BPM can achieve low overpotentials at high current density operation even when integrated within a 6 cm^2 active area electrodialysis flow cell with saltwater conditions relevant to DOC. These results indicate excellent mechanical stability, as well as favorable layer adhesion at high current densities and low overpotentials. In addition to analyzing the BPM experimentally, continuum-level simulations were conducted to investigate the mechanisms of WD occurring over the GrOx catalyst. The modeling revealed that WD in GrOx BPMs is both electric-field enhanced and catalyst-surface-mediated.[47−49] Collectively, the experimental results and simulations establish the industrial viability of the GrOx-catalyzed, asymmetric BPM and provide insights into the mechanisms of WD over oxide-based catalysts.

Figure 1 illustrates the layers and chemical structures of the GrOx-catalyzed, asymmetric BPM, along with relevant WD reaction pathways (Figure 1A), a cross-sectional SEM of the BPM layers (Figure 1B), and a picture of the fully assembled BPM (Figure 1C). Owing to its thin AEL and GrOx catalyst, the BPM was designed to overcome water transport limitations and enable operation at high current densities (≥500 mA cm^{-2}) in a freestanding environment, typically unattainable with commercial, freestanding BPMs.[46] Polarization curves for the best performing GrOx catalyzed, asymmetric BPM compared to the commercial Fumasep BPM, as tested in a freestanding electrodialysis flow configuration, are presented in Figure 2A. The GrOx catalyzed, asymmetric BPM outperformed the commercially available Fumasep BPM in all current density regions, where the performance of the Fumasep BPM became significantly limited by either water transport or WD kinetics at current density >300 mA cm^{-2}. Figure 2B demonstrates that the dominant contribution to BPM voltage is the thermodynamic potential required for WD, indicating that WD is occurring close to the thermodynamic minimum. Remarkably, even at 1 A cm^{-2}, the calculated overpotential is <250 mV.

Total overpotential, defined as the sum of contributions due to WD kinetics, membrane resistance, and solution resistance, at 100, 500, and 1000 mA cm^{-2} were calculated for state-of-the-art BPMs in literature.[2,13,17,38−40,43,45,51] Thermodynamic

https://doi.org/10.1021/acsenergylett.4c01662
ACS Energy Lett. 2024, 9, 5596−5605

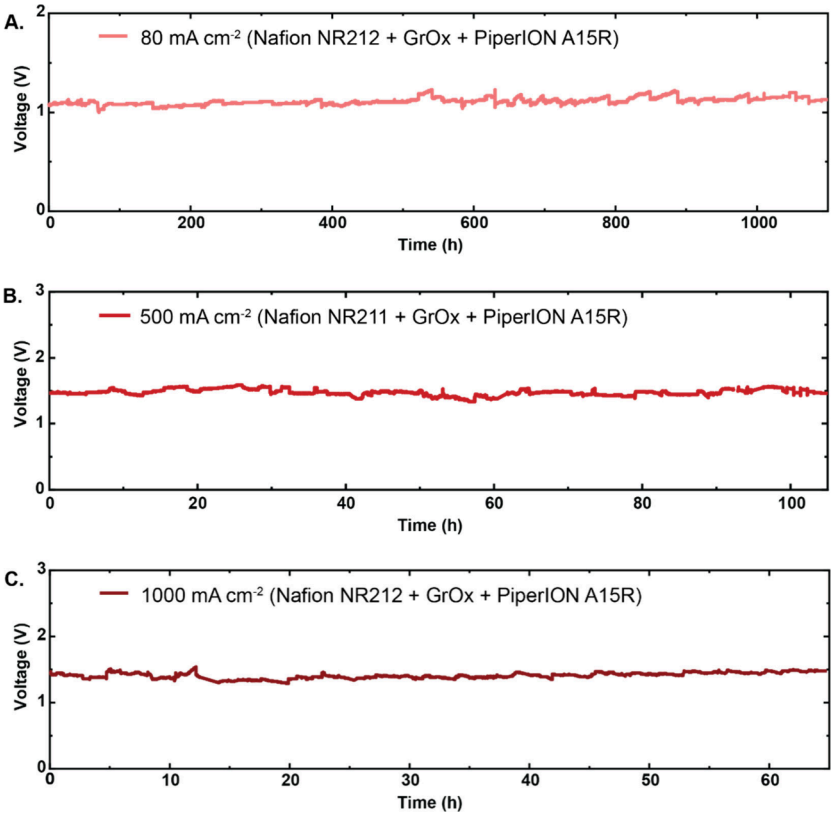

Figure 3. Voltage stability of the BPMs over time after stabilization at (A) 80 mA cm^{-2}, (B) 500 mA cm^{-2}, and (C) 1000 mA cm^{-2}. Note that it typically took approximately 1 h for formation and dispersion of bubbles to reach a steady state condition with minimal voltage fluctuation.

WD potentials at 100, 500, and 1000 mA cm^{-2} were calculated based on the testing environment described in each study (Section S2) and are presented in Table S1. The calculated total overpotentials were then compared to the GrOx catalyzed, asymmetric BPM in Figure 2C. Compared to other freestanding BPMs, the GrOx BPM demonstrates the lowest overpotentials across all measured current densities, 126 mV at 100 mA cm^{-2}, 144 mV at 500 mA cm^{-2}, and 242 mV at 1 A cm^{-2} compared to other BPMs in the freestanding configuration (Figure 2C).

The importance of the GrOx CL in obtaining low operating overpotentials is demonstrated in Figure S6, in which polarization curves of the asymmetric BPM with and without GrOx are compared. The total overpotential for high current density operation could be further reduced by making the CEL layer thinner or by increasing the ion-exchange capacity of both the CEL and AEL components. However, both changes would lead to an increase in co-ion leakage through the BPM, decreasing the efficiency for making acid and base.[42]

To achieve these impressive rates and efficiencies for BPM WD, optimization and characterization of the catalyst loading and morphology was performed, and an optimal mass loading of 225 μg cm^{-2} was determined (Section S5). Above this loading, electrochemical impedance spectroscopy capacitance data shows the loss of catalytically active surface area, potentially due to aggregation of the GrOx as confirmed by atomic force microscopy and optical microscopy. Such catalyst aggregation reduces available catalytically active sites and worsens contact between the AEL and CL. At loadings below the optimal value, the GrOx has not yet achieved complete coverage on the CEL, again reducing available sites for surface-mediated WD reactions.

Figure 2D compares the stability of the GrOx-catalyzed, asymmetric BPM with those reported for other BPMs (see Figure 3 for voltage vs time plots for the 3 stability points in Figure 2D). The data represents time to BPM failure, or end of reporting, at a specific current density. We note that most studies of BPMs in electrodialysis operation do not report stability data due to challenges associated with membrane delamination.[2,27,28]

Our asymmetric BPM exhibits excellent voltage stability at 80 mA cm^{-2} of 1100 h, at 500 mA cm^{-2} of 100 h, and at 1 A cm^{-2} of 60 h (Figure 3). The noise seen in the stability data is due to the formation and eventual release of dissolved gas bubbles on the surface of the BPM. In the measurements taken for the I−V curve (Figure 2A), the bubbles did not have sufficient time to build up and thus the voltage is lower. Work by Eisaman et al. has shown that in ED systems with trace amounts of carbon in the electrolyte in the form of dissolved inorganic carbon impurities (*e.g.*, (bi)carbonates), gaseous CO_2 can be evolved on the surface of the BPM by pH-swing degassing.[52] Similar phenomena could also explain the bubbles observed in this study, noting that CO_2 degassing would be enhanced by the high temperatures achieved by the BPM at high current densities (our thermal modeling suggests a temperature of 80 °C is reached at 1 A cm^{-2}, see Section S6). At this high temperature, CO_2 is less soluble in the electrolyte, and would degas at higher rates than at room temperature, potentially explaining the observed bubbling in our experiments. Future work is needed to examine in greater detail the nature of bubble formation on BPM surfaces.

https://doi.org/10.1021/acsenergylett.4c01662
ACS Energy Lett. 2024, 9, 5596−5605

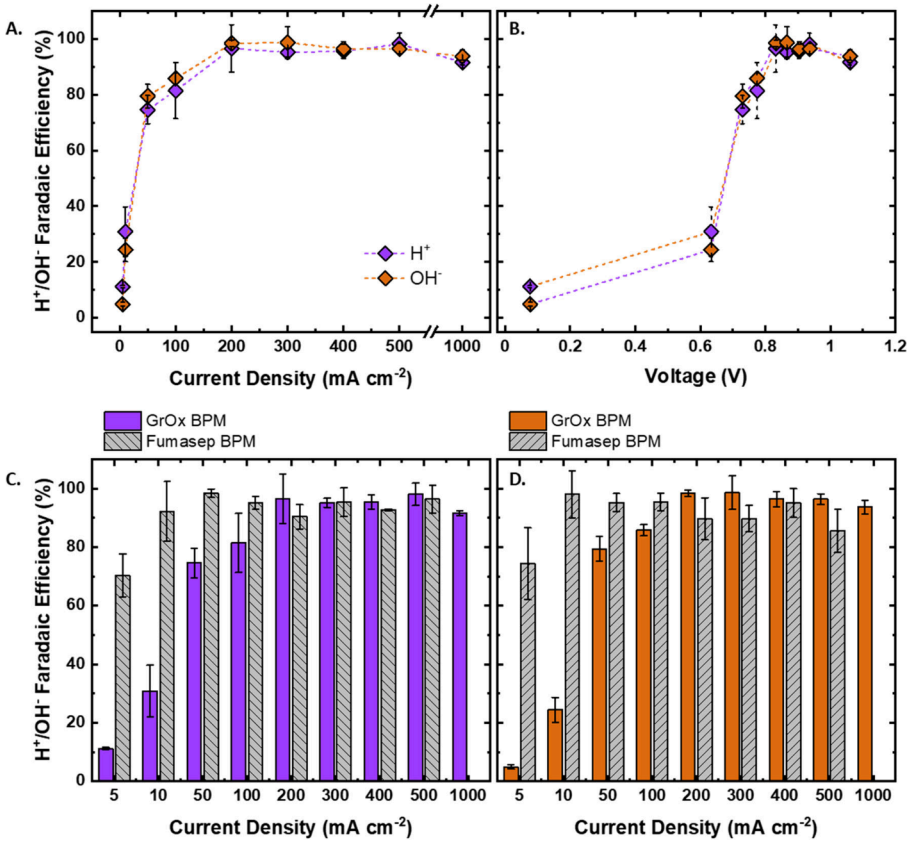

Figure 4. Faradaic efficiency for H^+ and OH^- vs (A) current density and (B) voltage for the best performing BPM (225 μg cm^{-2} GrOx loading) (GrOx BPM). Faradaic efficiency of (C) H^+ and (D) OH^- for the GrOx BPM compared to a Fumasep commercial BPM tested in the same environment.

While many BPMs suffer from poor mechanical adhesion, commonly associated with delamination of the AEL and CEL,[27,28] the Nafion CEL and PiperION AEL used in the BPM presented in this work have excellent adhesion likely due to observed strong electrostatic interactions. Furthermore, this membrane pairing has proven to be mechanically and chemically stable under reverse bias operation as well as in acidic and basic environments.[50,53−55] The addition of a WD catalyst to the BPM junction is typically detrimental to adhesion, necessitating the use of mechanical pressure during operation.[27,28] However, the stability observed for the asymmetric BPM reveals that GrOx only minimally interferes with the adhesion between Nafion and PiperION, and as fabricated, the layer-to-layer adhesion is sufficient to facilitate freestanding operation without the need for additional mechanical support.

T-peel tests were performed to better understand the adhesion between the CEL and AEL with and without a catalyst layer (Figure S10). The pristine BPM sample showed the strongest adhesion with the mean peel force being 0.071 N mm^{-1}. The graphene-oxide sample showed an order of magnitude weaker adhesion which was measured to be 0.0072 N mm^{-1}; however, we note that despite the decreased adhesion the experimental results clearly indicate it is sufficient for free-standing operation in the reported geometries. T-peel tests were also performed on BPMs with a TiO_2 catalyst, a commonly used WD catalyst in state-of-the-art BPMs.[13,38] Notably, the BPM fabricated with a TiO_2 catalyst layer was no longer adhered upon drying, thus the adhesion was so weak as to be nonexistent making a T-peel test impossible. This is illustrative of the unique freestanding capabilities of BPMs with GrOx catalysts compared to typical metal-oxide WD catalysts. This strong interfacial adhesion coupled with the high WD activity of GrOx unlocks a multitude of previously untenable BPM applications which require freestanding acid/base generation with high energy-efficiency. The strong adhesion can perhaps be attributed to interfacial van der Waals forces,[56] hydrogen bonding interactions[56,57] and other physiochemical properties. The amphiphilic nature of graphene oxide[57] could increase the adhesion forces with similarly amphiphilic ionomer membranes, as beneficial hydrophobic and hydrophilic interactions likely increase the adhesion energy. Alternatively, it is possible that the interfacial adhesion could result from GrOx being sufficiently conductive to screen the electrostatic interactions between the AEL and CEL, thus only minimally disrupting the adhesive forces.

The strong layer-to-layer adhesion of the BPM, resulting from the optimized combination of Nafion, PiperION, and GrOx, enables the BPM to overcome the stability limitations due to membrane delamination seen in many other systems.[27,28] The one stability challenge observed for the BPM was delamination due to warping of the Nafion membrane when the BPM was operated at 500 mA cm^{-2} and 1000 mA cm^{-2} for multiday stability tests. Operation at these high current densities for an extended period led to elevated temperatures (>40 °C) in the BPM (Section S6). Thus, we theorize that the elevated temperature over time causes the membranes to warp unevenly, delaminate at the junction, and eventually fail (Section S3).

https://doi.org/10.1021/acsenergylett.4c01662
ACS Energy Lett. 2024, 9, 5596−5605

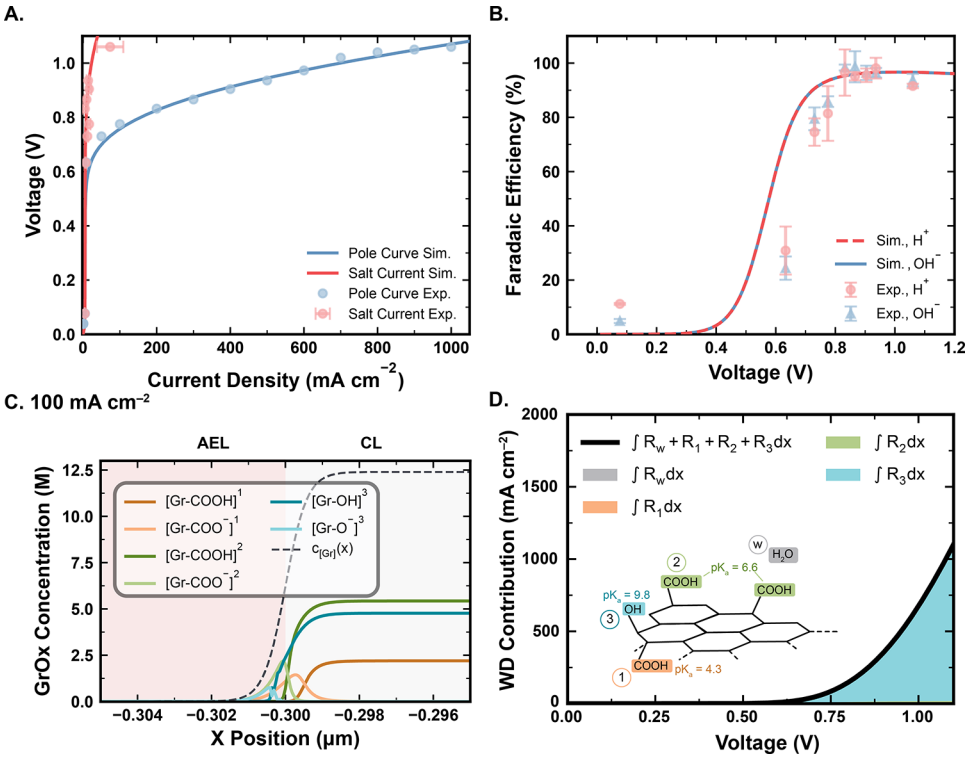

Figure 5. (A) Experimental (markers) and simulated (solid lines) polarization curves for total current density (blue) and salt-ion crossover (red). Salt crossover is calculated as described by Equation S86 in the Supporting Information. (B) Experimental (markers) and simulated (lines) FE of H^+ and OH^- generation by the BPM in the catholyte and anolyte, respectively. (C) Concentration profiles of GrOx species at the catalytic AEL|CL interface where the bulk of WD occurs for an operating current density of 100 mA cm^{-2}. (D) Breakdown of WD current density due to various WD pathways (see Figure 1A) integrated within the BPM CL. Orange area represents contribution to WD by R_1. Green area represents contribution to WD by R_2. Blue area represents contribution to WD by R_3. Gray area represents contribution to WD by the intrinsic WD pathway.

To show that the GrOx catalyzed, asymmetric BPM is functional beyond the lab-scale (1 cm^2) diagnostic electrodialysis cell, the BPM was scaled to have an active area of 6 cm^2 (full size of the BPM = 35 cm^2) and tested in an electrodialysis cell stack (Figure S11A-B), analogous with devices for industrial acid and base generation. Figure S11C shows calculated voltage contributions at multiple current densities for each layer of the cell stack compared to the experimentally measured polarization curve for the BPM tested in the cell stack.

In the operation of the one-cell BPM-ED stack, the total stack voltage to achieve a current density of 200 mA cm^{-2} was approximately 6 V, corresponding to a per-BPM voltage of 3 V. This voltage requirement is quite large and will need to be reduced for commercial application. Our applied voltage analysis (Figure S11C) suggests that most of the voltage losses arise not from the BPM, but rather from losses through the ion exchange membranes in the repeating unit cell. Hence, future work in scaling these BPM systems will require not only optimization of the BPM, but also optimization of the reactor itself and the components within it. Additionally, addressing concentration polarization and uneven current distributions in the BPM-ED cell at larger scales will be investigated in future work. Furthermore, at larger membrane areas, beyond what is demonstrated herein, mechanical reinforcement of the BPM may be required to prevent buckling and delamination.

To demonstrate translatability of the developed BPM to compressed MEA systems, an experiment was conducted to assess the performance of the GrOx catalyzed, asymmetric BPM for water electrolysis (Figure S51). The BPM performs quite well in the reactor, achieving 1 A cm^{-2} of water electrolysis at 2.5 V, on par with other recent demonstrations of high-performance BPM water electrolyzers.[37,58] We note that these measurements were not 4-probe measurements, so kinetic losses associated with the working electrodes may be convoluted with the measured potentials. Future work should seek to optimize GrOx BPMs and the reactors that contain them for water electrolysis, potentially using solid-state 4-probe measurements like those developed by Chen et al. to more accurately isolate and evaluate the GrOx BPM performance in this context.[36]

In addition to exhibiting scalability, low overpotentials, and exceptional stability at high current densities, the GrOx-catalyzed, asymmetric BPM exhibits excellent Faradaic efficiencies (FEs, defined as the efficiency of the applied electronic current to generate protons and hydroxides via WD) for acid and base production at >200 mA cm^{-2} (Figure 4A). Because of co-ion leakage through the thin AEL, FEs for H^+ and OH^- generation were low (~80% and lower) at operating current densities <200 mA cm^{-2} (or <0.8 V, Figure 4B). However, at current densities of >200 mA cm^{-2} (>0.8 V), the FEs for H^+ and OH^- generation were ~95%. This indicates that most of the current flowing through the cell is used to generate acid and base, as desired for the use of a BPM for DAC and DOC.

We note that the FE is low at lower current densities (<200 mA cm^{-2}). This is due to the trade-off associated with thinning the AEL. The thin AEL allows for the achievement of higher

https://doi.org/10.1021/acsenergylett.4c01662
ACS Energy Lett. 2024, 9, 5596−5605

current densities by improving water transport to the CL, but also enables greater crossover of co-ions from the external electrolyte. Due to the emphasis in this study on high-current density operation due to the techno-economic benefits of such operation, we choose to adopt a thin AEL.[59] However, for operation at lower current densities, thicker AELs may be necessary.

To elucidate the mechanism of WD within the BPM, as well as the sensitivity of the BPM performance to CL properties, a continuum-level model of the BPM was developed. The model employs a continuum representation of mass conservation in which the species fluxes were defined by the Poisson−Nernst−Planck equations and homogeneous-phase bulk reactions in the BPM domain (i.e., WD) were described by mass-action chemical kinetics with electric-field enhancement (See Section S7 for model physics). Using only three semiempirical fit parameters (Table S7), the model properly predicts polarization behavior of the GrOx catalyzed, asymmetric BPM, salt-crossover current density, and FE for acid−base generation (Figure 5A−B). The model was also able to define local pH and electrostatic potential profiles within the BPM and CL domains, demonstrating how the pH gradient within the BPM develops as current density increases (Figure S35). Interestingly, it can be observed that most of the pH and applied potential gradient occurs at the AEL-CL interface, suggesting that WD occurs primarily at this interface.

Analysis of the local electric field within the BPM CL reveals that the maximum in the electric field at the AEL-CL interface (Figure S39−40) coincides with the maximum rate of WD via the Second Wien Effect (Figure S41−42). The local maximum in electric field can be explained by examining the concentration profiles of the GrOx functional groups within the CL (Figure 5C and Figures S36−S38). Local generation of OH^- anions at the AEL-CL interface causes the most acidic GrOx functional groups (i.e., carboxylic groups) to deprotonate rapidly, resulting in a large buildup of negative charge, which, in turn, enhances the local electric field and accelerates WD chemistry via the Second Wien Effect. This finding is consistent with prior studies that suggest that the role of the catalyst is to develop surface charges that enhance the electric field and drive WD.[34,41,60] Examination of alternative WD pathways (Equations S40−S45, Figure 1A) shows that WD occurs predominantly via the reaction of H_2O with the least acidic GrOx functional groups (i.e., phenolic groups) (Figure 5D and Figure S43). The occurrence of WD at substantial rates by a catalyzed pathway has not been theoretically or experimentally reported before, as most prior simulations of WD observe that uncatalyzed WD is dominant, and that the role of the catalyst is solely to assist in forming the electric field.[34,41,60] By contrast, these simulations show that the more acidic carboxylate GrOx sites (type 1 and 2) serve to enhance the electric field and the least acidic phenolic GrOx sites (type 3), still present in >2 M concentrations at 100 mA cm^{-2} (Figure 5C), provide surface-catalyzed paths for WD that are faster than uncatalyzed WD in the bulk (Figure 5D). Collectively, the model shows that WD over GrOx catalysts is both electric-field and catalytically enhanced, because the diversity of pK_as across the surface sites on GrOx enables differing functionality for these sites depending on their pK_a.

To determine the extent to which the pK_a of different acidic groups in the CL affects the rate of WD, simulations of the BPM were carried out in which all sites in the CL were set to a single pK_a value equal to that of one of the pK_as associated with phenolic and carboxylic groups in GrOx (i.e., either pK_a = 4.3, 6.6, or 9.8). These single-site simulations (Figures S44−S46) were found to be consistent with those reported by Lin et al., who found that as the pK_a of the catalyst decreases, its WD performance improves because the acidic groups on the catalyst dissociate more readily, thereby enhancing the electric field and accelerating the rate-limiting step in WD.[41] For low pK_a (4.3 or 6.6) functional groups, WD occurs primarily via the electric-field-enhanced process, and catalyzed WD does not occur to a significant extent because of the lack of neutral sites at the AEL-CL interface (Figure S46).[41,60] Conversely, for higher pK_a (9.8) functional groups, catalyzed WD becomes the dominant reaction pathway, because the pK_a is sufficiently large to prevent full deprotonation. However, because there is substantially less negative charge at the AEL-CL interface in this case, the electric field, and thus the simulated rates of WD, are significantly lower. Intriguingly, single-site simulations demonstrate that a diversity of sites is necessary to enable the observed performance, as none of the single-site simulations performs as well as the base-case containing both −COOH and −OH sites (Figure S46). This result underscores that the coexistence of multiple sites on the GrOx facilitates the passage of WD through a surface-mediated and field-enhanced mechanism that occurs at an accelerated rate compared to field-enhanced WD of bulk water. Finally, we highlight that the dispersity of sites (*e.g.,* the fraction of −COOH and −OH sites) may change within the BPM junction environment. Hence, we performed sensitivity analysis for interlayer GrOx catalysts of arbitrary dispersity, demonstrating that the proposed mechanism can reproduce experimental results regardless of the distribution of sites present in the GrOx CL, as long as those sites have sufficient diversity in their pK_as (Figures S47−S48).

In conclusion, this study reports the successful development of a GrOx catalyzed, asymmetric BPM that overcomes water transport limitations and operates in reverse bias at high current density and low overpotentials, with high energy-efficiencies for acid and base production. Evaluation of this BPM for electrodialysis demonstrated stable freestanding operation for 1100 h at 80 mA cm^{-2}, >100 h at 500 mA cm^{-2}, and >60 h at 1 A cm^{-2}. Additionally, at an applied current density of 1 A cm^{-2}, the BPM exhibits an overpotential of only 242 mV and a FE for acid and base generation near unity. Additionally, the combination of AEL, CEL, and catalyst (PiperION, Nafion, and GrOx, respectively) chosen for the BPM enables interfacial adhesion at the BPM junction, which contributes to its long-term stability. Initial testing of the BPM in an electrodialysis cell stack with a scaled active area of 6 cm^2 also demonstrated high current density operation at low voltage and suggests an opportunity to unlock a large application-space that necessitates freestanding BPMs.

The performance of the BPM was optimized by varying the loading of the GrOx catalyst, where insufficient loading resulted in incomplete coverage of the GrOx, and excessive loading led to the loss of active sites to catalyst aggregation. Furthermore, continuum-level modeling of the BPM closely matches the experimentally measured polarization curves and FEs. These simulations revealed that high concentrations of both low and high pK_a deprotonation sites in the GrOx CL enhance the electric field at the AEL-CL interface and provide alternative, surface-mediated pathways for WD that are accelerated compared to bulk WD. This analysis provides a potential explanation for the exceptional performance of the

https://doi.org/10.1021/acsenergylett.4c01662
ACS Energy Lett. 2024, 9, 5596−5605

GrOx catalyzed, asymmetric BPM. In summary, this work demonstrates an efficient, freestanding BPM that can be readily employed in a wide array of electrochemical technologies in which operation with high current densities and low voltages is desirable, and provides new fundamental insights into the mechanisms of WD over oxide-based catalysts with well-defined pK_as.

■ ASSOCIATED CONTENT

Supporting Information

The Supporting Information is available free of charge at https://pubs.acs.org/doi/10.1021/acsenergylett.4c01662.

Materials and methods, experimental design and analysis, membrane stability, testing in electrodialysis stack, characterization and analysis of GrOx loading, cell and membrane temperature model, computational methods, additional modeling, titration details, supplemental figures, and water electrolysis data (PDF)

■ AUTHOR INFORMATION

Corresponding Authors

Harry A. Atwater − *Division of Engineering and Applied Science, California Institute of Technology, Pasadena, California 91125, United States;* orcid.org/0000-0001-9435-0201; Email: haa@caltech.edu

Chengxiang Xiang − *Division of Engineering and Applied Science, California Institute of Technology, Pasadena, California 91125, United States;* orcid.org/0000-0002-1698-6754; Email: cxx@caltech.edu

Authors

Éowyn Lucas − *Division of Engineering and Applied Science, California Institute of Technology, Pasadena, California 91125, United States*

Justin C. Bui − *Department of Chemical and Biomolecular Engineering, University of California, Berkeley, Berkeley, California 94720, United States; Chemical Sciences Division, Lawrence Berkeley National Laboratory, Berkeley, California 94720, United States;* orcid.org/0000-0003-4525-957X

Timothy Nathan Stovall − *Department of Chemistry, University of California, Berkeley, Berkeley, California 94720, United States; Energy Technologies Area, Lawrence Berkeley National Laboratory, Berkeley, California 94720, United States*

Monica Hwang − *Division of Engineering and Applied Science, California Institute of Technology, Pasadena, California 91125, United States*

Kaiwen Wang − *Division of Engineering and Applied Science, California Institute of Technology, Pasadena, California 91125, United States*

Emily R. Dunn − *Division of Chemistry and Chemical Engineering, California Institute of Technology, Pasadena, California 91125, United States*

Ellis Spickermann − *Division of Engineering and Applied Science, California Institute of Technology, Pasadena, California 91125, United States*

Lily Shiau − *Division of Engineering and Applied Science, California Institute of Technology, Pasadena, California 91125, United States*

Ahmet Kusoglu − *Energy Technologies Area, Lawrence Berkeley National Laboratory, Berkeley, California 94720, United States;* orcid.org/0000-0002-2761-1050

Adam Z. Weber − *Energy Technologies Area, Lawrence Berkeley National Laboratory, Berkeley, California 94720, United States;* orcid.org/0000-0002-7749-1624

Alexis T. Bell − *Department of Chemical and Biomolecular Engineering, University of California, Berkeley, Berkeley, California 94720, United States; Chemical Sciences Division, Lawrence Berkeley National Laboratory, Berkeley, California 94720, United States;* orcid.org/0000-0002-5738-4645

Shane Ardo − *Department of Chemistry, Department of Chemical & Biomolecular Engineering, and Department of Materials Science & Engineering, University of California Irvine, Irvine, California 92697, United States;* orcid.org/0000-0001-7162-6826

Complete contact information is available at: https://pubs.acs.org/10.1021/acsenergylett.4c01662

Author Contributions

‡É.L. and J.C.B. contributed equally. É.L. developed five chamber BPM testing cell, designed and fabricated BPMs, performed electrochemical experiments, characterizations, and data analysis. J.C.B. performed data interpretation, figure development, and all continuum model calculations. T.N.S and fabricated BPMs and porous transport electrodes, performed zero-gap water electrolyzer testing, and T-peel tests. M.H. developed thin cell electrodialysis stack and testing of BPM in the stack. K.W. performed temperature environment simulations and figure development. E.R.D. and E.S. conducted electrodialysis measurements and assisted with reviewer responses and MS/SI updates. L.S. performed XPS measurements. A.K. assisted with T-peel test methods and measurements. A.T.B., A.Z.W., S.A., H.A.A., and C.X. supervised the project. All authors discussed results and participated in the preparation of the manuscript.

Notes

The authors declare the following competing financial interest(s): Harry Atwater and CX Xiang are co-founders of Captura Corporation, which has licensed technology reported in this paper.

■ ACKNOWLEDGMENTS

This work (materials development, fabrication, and characterization) was primarily supported as part of United States Department of Energy, Advanced Research Projects Agency−Energy (ARPA-e) under contract number DE-AR0001407 (É.L., M.H., K.W., E.R.D., S.A., H.A.A, C.X.). Computational work was supported by the Liquid Sunlight Alliance, which is supported by the US Department of Energy, Office of Science, Office of Basic Energy Sciences, Fuels from Sunlight Hub under award number DE-SC0021266 (J.C.B., E.S., L.S., A.T.B., A.Z.W.). J.C.B. would like to acknowledge support from the National Defense Science and Engineer Graduate Fellowship (NDSEG) supported by the Army Research Office (ARO). T.N.S. and E.R.D. acknowledge support from the National Science Foundation Graduate Research Fellowship (NSFGRFP) under Grant No. DGE 2146752 and No. 2139433, respectively.

■ REFERENCES

(1) Thiele, S.; Mayerhöfer, B.; McLaughlin, D.; Böhm, T.; Hegelheimer, M.; Seeberger, D. Bipolar Membrane Electrode Assemblies for Water Electrolysis. *ACS Appl. Energy Mater.* **2020**, *3* (10), 9635−9644.

(2) Ge, Z.; Shehzad, M. A.; Yang, X.; Li, G.; Wang, H.; Yu, W.; Liang, X.; Ge, X.; Wu, L.; Xu, T. High-Performance Bipolar Membrane for Electrochemical Water Electrolysis. *J. Membr. Sci.* **2022**, *656*, 120660.
(3) Thiele, S.; Mayerhöfer, B.; Mayerhöfer, M.; Ehelebe, K.; Speck, F. D.; Bierling, M.; Bender, J.; Kerres, J. A.; Mayrhofer, K. J. J.; Cherevko, S.; Peach, R. On the Effect of Anion Exchange Ionomer Binders in Bipolar Electrode Membrane Interface Water Electrolysis. *J. Mater. Chem. A Mater.* **2021**, *9* (25), 14285.
(4) Wang, X.; Rossi, R.; Yan, Z.; Yang, W.; Hickner, M. A.; Mallouk, T. E.; Logan, B. E. Balancing Water Dissociation and Current Densities To Enable Sustainable Hydrogen Production with Bipolar Membranes in Microbial Electrolysis Cells. *Environ. Sci. Technol.* **2019**, *53*, 14761−14768.
(5) Zhou, X.; Liu, R.; Sun, K.; Chen, Y.; Verlage, E.; Francis, S. A.; Lewis, N. S.; Xiang, C. Solar-Driven Reduction of 1 Atm of CO2 to Formate at 10% Energy-Conversion Efficiency by Use of a TiO2-Protected III-V Tandem Photoanode in Conjunction with a Bipolar Membrane and a Pd/C Cathode. *ACS Energy Lett.* **2016**, *1* (4), 764−770.
(6) Digdaya, I. A.; Sullivan, I.; Lin, M.; Han, L.; Cheng, W. H.; Atwater, H. A.; Xiang, C. A Direct Coupled Electrochemical System for Capture and Conversion of CO2 from Oceanwater. *Nat. Commun.* **2020**, *11* (1), 1−10.
(7) Xu, J.; Zhong, G.; Li, M.; Zhao, D.; Sun, Y.; Hu, X.; Sun, J.; Li, X.; Zhu, W.; Li, M.; Zhang, Z.; Zhang, Y.; Zhao, L.; Zheng, C.; Sun, X. Review on Electrochemical Carbon Dioxide Capture and Transformation with Bipolar Membranes. *Chin. Chem. Lett.* **2023**, *34*, 108075.
(8) Jin, S.; Wu, M.; Jing, Y.; Gordon, R. G.; Aziz, M. J. Low Energy Carbon Capture via Electrochemically Induced PH Swing with Electrochemical Rebalancing. *Nature Communications 2022 13:1* **2022**, *13* (1), 1−11.
(9) Liu, Y.; Lucas, É.; Sullivan, I.; Li, X.; Xiang, C. Challenges and Opportunities in Continuous Flow Processes for Electrochemically Mediated Carbon Capture. *iScience* **2022**, *25* (10), No. 105153.
(10) *Climate Change 2022: Mitigation of Climate Change*. https://www.ipcc.ch/report/ar6/wg3/?itid=lk_inline_enhanced-template (accessed 2022-12-04).
(11) Armstrong McKay, D. I.; Staal, A.; Abrams, J. F.; Winkelmann, R.; Sakschewski, B.; Loriani, S.; Fetzer, I.; Cornell, S. E.; Rockström, J.; Lenton, T. M. Exceeding 1.5°C Global Warming Could Trigger Multiple Climate Tipping Points. *Science (1979)* **2022**, *377* (6611), eabn7950 DOI: 10.1126/science.abn7950.
(12) Rogelj, J.; Popp, A.; Calvin, K. V.; Luderer, G.; Emmerling, J.; Gernaat, D.; Fujimori, S.; Strefler, J.; Hasegawa, T.; Marangoni, G.; Krey, V.; Kriegler, E.; Riahi, K.; Van Vuuren, D. P.; Doelman, J.; Drouet, L.; Edmonds, J.; Fricko, O.; Harmsen, M.; Havlík, P.; Humpenöder, F.; Stehfest, E.; Tavoni, M. Scenarios towards Limiting Global Mean Temperature Increase below 1.5 °C. *Nature Climate Change 2018 8:4* **2018**, *8* (4), 325−332.
(13) Oener, S. Z.; Twight, L. P.; Lindquist, G. A.; Boettcher, S. W. Thin Cation-Exchange Layers Enable High-Current-Density Bipolar Membrane Electrolyzers via Improved Water Transport. *ACS Energy Lett.* **2021**, *6* (1), 1−8.
(14) Vermaas, D. A.; Wiegman, S.; Nagaki, T.; Smith, W. A. Ion Transport Mechanisms in Bipolar Membranes for (Photo)-Electrochemical Water Splitting. *Sustain Energy Fuels* **2018**, *2* (9), 2006−2015.
(15) Sun, K.; Liu, R.; Chen, Y.; Verlage, E.; Lewis, N. S.; Xiang, C. A Stabilized, Intrinsically Safe, 10% Efficient, Solar-Driven Water-Splitting Cell Incorporating Earth-Abundant Electrocatalysts with Steady-State PH Gradients and Product Separation Enabled by a Bipolar Membrane. *Adv. Energy Mater.* **2016**, *6* (13), 1600379.
(16) Vargas-Barbosa, N. M.; Geise, G. M.; Hickner, M. A.; Mallouk, T. E. Assessing the Utility of Bipolar Membranes for Use in Photoelectrochemical Water-Splitting Cells. *ChemSusChem* **2014**, *7* (11), 3017−3020.
(17) Powers, D.; Mondal, A. N.; Yang, Z.; Wycisk, R.; Kreidler, E.; Pintauro, P. N. Freestanding Bipolar Membranes with an Electrospun Junction for High Current Density Water Splitting. *Cite This: ACS Appl. Mater. Interfaces* **2022**, *14*, 36092−36104.
(18) Lucas, É.; Han, L.; Sullivan, I.; Atwater, H. A.; Xiang, C. Measurement of Ion Transport Properties in Ion Exchange Membranes for Photoelectrochemical Water Splitting. *Front Energy Res.* **2022**, *10*, 1383.
(19) McDonald, M. B.; Bruce, J. P.; McEleney, K.; Freund, M. S. Reduced Graphene Oxide Bipolar Membranes for Integrated Solar Water Splitting in Optimal PH. *ChemSusChem* **2015**, *8* (16), 2645−2654.
(20) Erans, M.; Sanz-Pérez, E. S.; Hanak, D. P.; Clulow, Z.; Reiner, D. M.; Mutch, G. A. Direct Air Capture: Process Technology, Techno-Economic and Socio-Political Challenges. *Energy Environ. Sci.* **2022**, *15*, 1360.
(21) Ozkan, M.; Nayak, S. P.; Ruiz, A. D.; Jiang, W. Current Status and Pillars of Direct Air Capture Technologies. *iScience* **2022**, *25* (4), 103990.
(22) Fasihi, M.; Efimova, O.; Breyer, C. Techno-Economic Assessment of CO 2 Direct Air Capture Plants. *J. Clean Prod* **2019**, *224*, 957−980.
(23) Jayarathna, C.; Maelum, M.; Karunarathne, S.; Andrenacci, S.; Haugen, H. A. Review on Direct Ocean Capture (DOC) Technologies. *GHGT-16* **2022**. DOI: 10.2139/ssrn.4282969
(24) Sabatino, F.; Gazzani, M.; Gallucci, F.; Van Sint Annaland, M. Modeling, Optimization, and Techno-Economic Analysis of Bipolar Membrane Electrodialysis for Direct Air Capture Processes. *Ind. Eng. Chem. Res.* **2022**, *61* (34), 12668−12679.
(25) Sabatino, F.; Gazzani, M.; Gallucci, F.; van Sint Annaland, M. Modeling, Optimization, and Techno-Economic Analysis of Bipolar Membrane Electrodialysis for Direct Air Capture Processes. *Ind. Eng. Chem. Res.* **2022**, *2022* (34), 12668−12679.
(26) Sabatino, F.; Mehta, M.; Grimm, A.; Gazzani, M.; Gallucci, F.; Kramer, G. J.; Van Sint Annaland, M. Evaluation of a Direct Air Capture Process Combining Wet Scrubbing and Bipolar Membrane Electrodialysis. *Ind. Eng. Chem. Res.* **2020**, *59* (15), 7007−7020.
(27) Pärnamäe, R.; Mareev, S.; Nikonenko, V.; Melnikov, S.; Sheldeshov, N.; Zabolotskii, V.; Hamelers, H. V. M.; Tedesco, M. Bipolar Membranes: A Review on Principles, Latest Developments, and Applications. *J. Membr. Sci.* **2021**, *617*, 118538.
(28) Giesbrecht, P. K.; Freund, M. S. Recent Advances in Bipolar Membrane Design and Applications. *Chem. Mater.* **2020**, *32* (19), 8060−8090.
(29) Schulte, L.; White, W.; Renna, L. A.; Ardo, S. Turning Water into a Protonic Diode and Solar Cell via Doping and Dye Sensitization. *Joule* **2021**, *5* (9), 2380−2394.
(30) Bui, J. C.; Lees, E. W.; Marin, D. H.; Stovall, T. N.; Chen, L.; Kusoglu, A.; Nielander, A. C.; Jaramillo, T. F.; Boettcher, S. W.; Bell, A. T.; Weber, A. Z. Multi-Scale Physics of Bipolar Membranes in Electrochemical Processes. *Nature Chemical Engineering* **2024**, *1* (1), 45−60.
(31) Mafé, S.; Ramírez, P.; Alcaraz, A. Electric Field-Assisted Proton Transfer and Water Dissociation at the Junction of a Fixed-Charge Bipolar Membrane. *Chem. Phys. Lett.* **1998**, *294* (4−5), 406−412.
(32) Alcaraz, A.; Ramírez, P.; Mafé, S.; Holdik, H.; Bauer, B. Ion Selectivity and Water Dissociation in Polymer Bipolar Membranes Studied by Membrane Potential and Current-Voltage Measurements. *Polymer (Guildf)* **2000**, *41* (17), 6627−6634.
(33) Strathmann, H.; Krol, J. J.; Rapp, H. J.; Eigenberger, G. Limiting Current Density and Water Dissociation in Bipolar Membranes. *J. Membr. Sci.* **1997**, *125* (1), 123−142.
(34) Bui, J. C.; Corpus, K. R. M.; Bell, A. T.; Weber, A. Z. On the Nature of Field-Enhanced Water Dissociation in Bipolar Membranes. *J. Phys. Chem. C* **2021**, *125* (45), 24974−24987.
(35) Aritomi, T.; van den Boomgaard, T.; Strathmann, H. Current-Voltage Curve of a Bipolar Membrane at High Current Density. *Desalination* **1996**, *104* (1−2), 13−18.

(36) Chen, L.; Xu, Q.; Boettcher, S. W. Kinetics and Mechanism of Heterogeneous Voltage-Driven Water-Dissociation Catalysis. *Joule* **2023**, *7* (8), 1867−1886.
(37) Marin, D. H.; Perryman, J. T.; Hubert, M. A.; Lindquist, G. A.; Chen, L.; Aleman, A. M.; Kamat, G. A.; Niemann, V. A.; Stevens, M. B.; Regmi, Y. N.; Boettcher, S. W.; Nielander, A. C.; Jaramillo, T. F. Hydrogen Production with Seawater-Resilient Bipolar Membrane Electrolyzers. *Joule* **2023**, *7* (4), 765−781.
(38) Oener, S. Z.; Foster, M. J.; Boettcher, S. W. Accelerating Water Dissociation in Bipolar Membranes and for Electrocatalysis. *Science (1979)* **2020**, *369* (6507), 1099−1103.
(39) Shen, C.; Wycisk, R.; Pintauro, P. N. High Performance Electrospun Bipolar Membrane with a 3D Junction. *Energy Environ. Sci.* **2017**, *10* (6), 1435−1442.
(40) Hohenadel, A.; Powers, D.; Wycisk, R.; Adamski, M.; Pintauro, P.; Holdcroft, S. Electrochemical Characterization of Hydrocarbon Bipolar Membranes with Varying Junction Morphology. *ACS Appl. Energy Mater.* **2019**, *2* (9), 6817−6824.
(41) Lin, M.; Digdaya, I. A.; Xiang, C. Modeling the Electrochemical Behavior and Interfacial Junction Profiles of Bipolar Membranes at Solar Flux Relevant Operating Current Densities. *Sustain Energy Fuels* **2021**, *5* (7), 2149−2158.
(42) Bui, J. C.; Digdaya, I.; Xiang, C.; Bell, A. T.; Weber, A. Z. Understanding Multi-Ion Transport Mechanisms in Bipolar Membranes. *ACS Appl. Mater. Interfaces* **2020**, *12* (47), 52509−52526.
(43) Al-Dhubhani, E.; Swart, H.; Borneman, Z.; Nijmeijer, K.; Tedesco, M.; Post, J. W.; Saakes, M. Entanglement-Enhanced Water Dissociation in Bipolar Membranes with 3D Electrospun Junction and Polymeric Catalyst. *ACS Appl. Energy Mater.* **2021**, *4* (4), 3724−3736.
(44) Hohenadel, A.; Gangrade, A. S.; Holdcroft, S. Spectroelectrochemical Detection of Water Dissociation in Bipolar Membranes. *ACS Appl. Mater. Interfaces* **2021**, *13* (38), 46125−46133.
(45) Yan, Z.; Zhu, L.; Li, Y. C.; Wycisk, R. J.; Pintauro, P. N.; Hickner, M. A.; Mallouk, T. E. The Balance of Electric Field and Interfacial Catalysis in Promoting Water Dissociation in Bipolar Membranes. *Energy Environ. Sci.* **2018**, *11* (8), 2235−2245.
(46) Xu, Z.; Liao, Y.; Pang, M.; Wan, L.; Xu, Q.; Zhen, Y.; Wang, B. A Chemically Interlocked Bipolar Membrane Achieving Stable Water Dissociation for High Output Ammonia Electrosynthesis. *Energy Environ. Sci.* **2023**, *16* (9), 3815−3824.
(47) Konkena, B.; Vasudevan, S. Understanding Aqueous Dispersibility of Graphene Oxide and Reduced Graphene Oxide through PK a Measurements. *J. Phys. Chem. Lett.* **2012**, *3*, 867−872.
(48) Orth, E. S.; Ferreira, J. G. L.; Fonsaca, J. E. S.; Blaskievicz, S. F.; Domingues, S. H.; Dasgupta, A.; Terrones, M.; Zarbin, A. J. G. PKa Determination of Graphene-like Materials: Validating Chemical Functionalization. *J. Colloid Interface Sci.* **2016**, *467*, 239−244.
(49) Ardo, S.; White, W.; Renna, L.; Bhide, R.; Schultz, L.; Phun, G. Membranes for Enhancing Rates of Water Dissociation and Water Formation. U.S. Patent WO 20210046423A1. February 18, 2021.
(50) Wang, J.; Zhao, Y.; Setzler, B. P.; Rojas-Carbonell, S.; Ben Yehuda, C.; Amel, A.; Page, M.; Wang, L.; Hu, K.; Shi, L.; Gottesfeld, S.; Xu, B.; Yan, Y. Poly(Aryl Piperidinium) Membranes and Ionomers for Hydroxide Exchange Membrane Fuel Cells. *Nat. Energy* **2019**, *4* (5), 392−398.
(51) McDonald, M. B.; Freund, M. S. Graphene Oxide as a Water Dissociation Catalyst in the Bipolar Membrane Interfacial Layer. *ACS Appl. Mater. Interfaces* **2014**, *6* (16), 13790−13797.
(52) Eisaman, M. D.; Alvarado, L.; Larner, D.; Wang, P.; Littau, K. A. CO 2 Desorption Using High-Pressure Bipolar Membrane Electrodialysis. *Energy Environ. Sci.* **2011**, *4* (10), 4031−4037.
(53) Luo, X.; Rojas-Carbonell, S.; Yan, Y.; Kusoglu, A. Structure-Transport Relationships of Poly(Aryl Piperidinium) Anion-Exchange Membranes: Eeffect of Anions and Hydration. *J. Membr. Sci.* **2020**, *598*, No. 117680.
(54) Thuc, V. D.; Cong Tinh, V. D.; Kim, D. Simultaneous Improvement of Proton Conductivity and Chemical Stability of Nafion Membranes via Embedment of Surface-Modified Ceria Nanoparticles in Membrane Surface. *J. Membr. Sci.* **2022**, *642*, No. 119990.
(55) Zhou, Y.; Yu, L.; Wang, J.; Liu, L.; Liang, F.; Xi, J. Rational Use and Reuse of Nafion 212 Membrane in Vanadium Flow Batteries. *RSC Adv.* **2017**, *7* (32), 19425−19433.
(56) Hu, R.; He, Y.; Huang, M.; Zhao, G.; Zhu, H. Strong Adhesion of Graphene Oxide Coating on Polymer Separation Membranes. *Langmuir* **2018**, *34* (36), 10569−10579.
(57) Jeong, J. T.; Choi, M. K.; Sim, Y.; Lim, J. T.; Kim, G. S.; Seong, M. J.; Hyung, J. H.; Kim, K. S.; Umar, A.; Lee, S. K. Effect of Graphene Oxide Ratio on the Cell Adhesion and Growth Behavior on a Graphene Oxide-Coated Silicon Substrate. *Scientific Reports 2016 6:1* **2016**, *6* (1), 1−10.
(58) Chen, L.; Xu, Q.; Oener, S. Z.; Fabrizio, K.; Boettcher, S. W. Design Principles for Water Dissociation Catalysts in High-Performance Bipolar Membranes. *Nature Communications 2022 13:1* **2022**, *13* (1), 1−10.
(59) Sabatino, F.; Gazzani, M.; Gallucci, F.; Van Sint Annaland, M. Modeling, Optimization, and Techno-Economic Analysis of Bipolar Membrane Electrodialysis for Direct Air Capture Processes. *Ind. Eng. Chem. Res.* **2022**, *61* (34), 12668−12679.
(60) Craig, N. P. Electrochemical Behavior of Bipolar Membranes, 2013. https://escholarship.org/uc/item/8058x81t (accessed 2022-12-28).

https://doi.org/10.1021/acsenergylett.4c01662
ACS Energy Lett. 2024, 9, 5596−5605